Acta Crystallographica Section B
Structural Science
ISSN 0108-7681

High-pressure experimental study on Rb_2S: anti-fluorite to Ni_2In-type phase transitions

David Santamaria-Perez,[a]* Angel Vegas,[b] Claus Muehle[c] and Martin Jansen[c]

[a]Departamento de Química Física I, Universidad Complutense de Madrid, Avda. Complutense s/n, Madrid E-28040, Spain, [b]Instituto de Química Física 'Rocasolano', CSIC, Serrano 119, Madrid 28006, Spain, and [c]Max-Planck Institut für Festkörperforschung, Heisenbergstrasse 1, Stuttgart 70569, Germany

Correspondence e-mail: dsantamaria@quim.ucm.es

Received 18 November 2010
Accepted 21 December 2010

The high-pressure behaviour of dirubidium sulfide, Rb_2S, with antifluorite-type structure under room conditions (space group $Fm\bar{3}m$) has been studied up to 8 GPa at room temperature using angle-dispersive X-ray powder diffraction in a diamond–anvil cell (DAC). X-ray measurements have allowed us to completely characterize two phase transitions upon compression: (i) to an anticotunnite-type structure (*Pnma*) at some pressure between 1 bar and 0.7 GPa, and (ii) to a Ni_2In-type structure ($P6_3/mmc$) at 2.6 GPa. A gradual transition from the *Pnma* to the $P6_3/mmc$ structures seems to occur between 2.6 and 4.5 GPa. These results are in excellent agreement with previous theoretical predictions. Strong luminescence is observed above 2.6 GPa (band maximum at 703 nm) when the transition to the Ni_2In-type phase starts to occur, the band maximum showing a non-linear blue shift with pressure. The observed sequence of phase transitions in Rb_2S is discussed in relation to the high-pressure structural behaviour of isomorphic sulfides and the structures are compared with the cationic arrays of their corresponding oxides (*e.g.* rubidium sulfate, in which the sulfide has been oxidized).

1. Introduction

The alkali-metal sulfides Li_2S, Na_2S, K_2S and Rb_2S are found to crystallize in the cubic antifluorite (*anti*-CaF_2-type) structure (May, 1936; Zintl *et al.*, 1934). Dirubidium sulfide, Rb_2S, in particular, was first synthesized by May in 1936 (May, 1936).

Pressure-induced phase transitions in fluorite-type to cotunnite-type compounds were found in several dihalogenides and dioxides (Beck, 1979; Brixner, 1976; Duclos *et al.*, 1988), and some of them further transform into post-cotunnite or Ni_2In-type structures. Similar high-pressure behaviour has also been found in antifluorite-type compounds, such as alkali sulfides. High-pressure experimental studies on M_2S sulfides (M = Li, Na and K) have recently been reported (Grzechnik *et al.*, 2000; Vegas *et al.*, 2001, 2002). In the case of Li_2S, at 12 GPa, antifluorite → anticotunnite was the only transition observed (Grzechnik *et al.*, 2000). In Na_2S a sequence of structural transformations along the path antifluorite → anticotunnite → Ni_2In-type occurs at pressures of *ca* 7 and 16 GPa (Vegas *et al.*, 2002). Finally, in K_2S a distorted Ni_2In-type structure was characterized at 6 GPa (Vegas *et al.*, 2001). Below this pressure, unknown phases seem to coexist. Thus, in these compounds there is a high-pressure phase-transition path that involves an increase of the cation coordination number from 8 in the antifluorite structure, through 9 in anticotunnite to 11 in Ni_2In-type structure.

Theoretical *ab initio* total-energy calculations carried out by Schön *et al.* allowed the high-pressure phases observed

experimentally in Li_2S, Na_2S and K_2S to be completely characterized, and the most likely phases that are expected to be stable below 100 GPa could be predicted for all alkali metal sulfides (Schön *et al.*, 2004). High-pressure structure candidates were identified with a global optimization on the enthalpy landscape of each particular chemical system. In this way total-energy calculations on Rb_2S proposed the anti-fluorite → anticotunnite → Ni_2In-type sequence of stable structures with increasing pressure.

The aim of this work is to study experimentally the structural stability of Rb_2S under pressure in order to confirm these theoretical predictions. Room-temperature angle-dispersive X-ray diffraction (ADXRD) measurements were carried out up to 8 GPa using a diamond–anvil cell (DAC). The diffraction experiments confirm the theoretical predictions, *i.e.* Rb_2S undergoing the double transition *anti*-CaF_2 → *anti*-$PbCl_2$ → Ni_2In-type at 0.7 and 4.5 GPa.

2. Experimental

Rb_2S was synthesized from stoichometric amounts of the elements, by heating them in an evacuated quarz ampoule at 623 K for 48 h. The extremely air-sensitive white powder obtained was identified to be pure Rb_2S using a Stoe X-ray powder diffractometer in the 2θ range 10–120° with monochromatic $K\alpha_1$ copper radiation. The polycrystalline Rb_2S sample was loaded into the diamond–anvil cell in an Ar atmosphere in a glove-box. High-pressure measurements on Rb_2S powder were performed in a modified Merrill–Bassett diamond–anvil cell (DAC) up to 8 GPa. The diamond anvils used have a culet size of 1 mm. The Rb_2S powder was placed in a 400 µm-diameter hole of the stainless steel gasket preindented to a thickness of 60 µm. No hydrostatic pressure-transmitting medium was used in order to avoid possible chemical reactions. Ruby chips evenly distributed in the pressure chamber were used to measure the pressure by the ruby fluorescence method (Mao *et al.*, 1986). Pressures measured in different ruby chips are within 0.1 GPa in the whole pressure range of the experiment. The diamond cell used for these experiments allows access to the angular range $4\theta = 50°$. Angle-dispersive X-ray diffraction measurements on Rb_2S have been carried out with a Xcalibur diffractometer (Oxford Diffraction Limited). The same set-up was used previously to successfully characterize the high-pressure (HP) phases of some ABO_4 compounds (Errandonea *et al.*, 2010; López-Solano *et al.*, 2010). X-ray diffraction patterns were obtained on a 135 mm Atlas CCD detector placed 110 mm from the sample using $K\alpha_1$:$K\alpha_2$ molybdenum radiation. The X-ray beam was collimated to a diameter of 300 µm. Exposure to the starting material in a 0.5 mm glass capillary was also obtained with this configuration. Exposure times were typically around 1 h 20 min. The observed intensities were integrated as a function of 2θ in order to give conventional, one-dimensional diffraction profiles. The *CrysAlis* software, Version 171.33.55 (Oxford Diffraction Limited), was used for data collection and the preliminary reduction of the data. The indexing and refinement of the powder patterns were performed using the *FULLPROF* (Rodríguez-Carvajal, 1993) and *POWDERCELL* (Nolze & Kraus, 1998) program packages.

Luminescence measurements were carried out using an optical set-up in which the sample was excited by a green 532 nm laser and the light emission spectra were collected by an AvaSpec spectrometer (Avantes, model 2048–2) in the wavelength range 180–1100 nm.

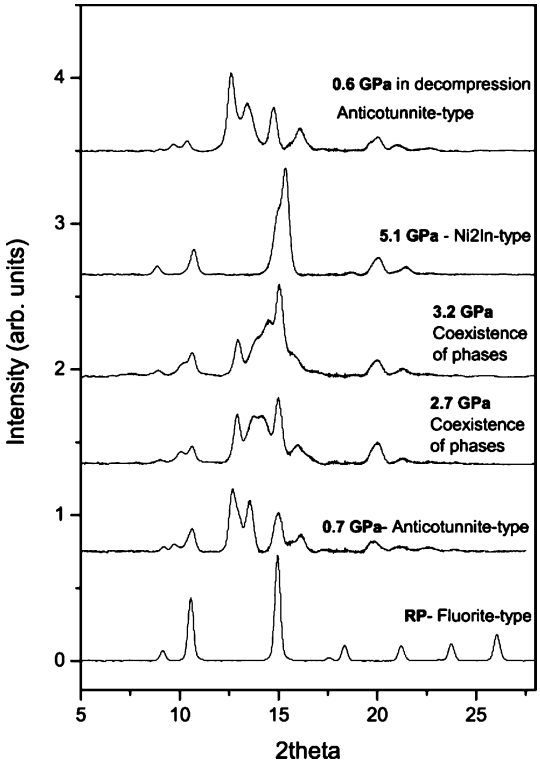

Figure 1
Selected X-ray powder diffraction patterns of Rb_2S at different pressures. Backgrounds are subtracted.

3. Results and discussion

The *in situ* ADXRD data of Rb_2S measured at different pressures are shown in Fig. 1. At room pressure the X-ray pattern corresponds to a cubic antifluorite-type structure (space group $Fm\bar{3}m$), with a lattice parameter of 7.726 (3) Å and unit-cell volume of 461.2 (3) Å^3 (Z = 4). The X-ray pattern completely changed at a pressure of 0.7 GPa, indicating the existence of a phase transition at near atmospheric pressure. No peaks of the initial antifluorite phase are present. The diffraction pattern of this high-pressure phase (phase II) has a larger number of reflections, suggesting a decrease in the crystal symmetry.

The peaks of the 0.7 GPa diffractogram could be indexed in an orthorhombic cell with lattice constants: a = 8.17 (1), b = 5.101 (6) and c = 9.96 (1) Å, V = 414.7(8) Å^3 and Z = 4. Therefore, this structure implies an approximated volume collapse of 9% at the transition. Phase II is stable up to at least 2 GPa. The systematic absences are consistent with the space

Table 1
Rb—S bond lengths (Å) in the coordination polyhedra around the S atoms.

The asterisks mark the Rb—S distances corresponding to the trigonal prisms in the anticotunnite-type and Ni_2In-type structures.

	Distances Rb—S
Anti-CaF_2-type phase (room pressure)	8 × 3.346 (3)
Anti-$PbCl_2$-type phase (0.7 GPa)	1 × 3.137 (5)
	2 × 3.296 (4)*
	1 × 3.349 (2)
	2 × 3.424 (4)*
	1 × 3.620 (6)
	2 × 3.771 (9)*
Ni_2In-type phase (5.1 GPa)	3 × 3.067 (7)
	2 × 3.405 (4)
	6 × 3.507 (5)*

group *Pnma* which corresponds to that of the *anti*-$PbCl_2$ structure. This structure model was refined by the Rietveld method, leading to the following atomic parameters: Rb1 [0.039 (1), 0.25, 0.1891 (4)], Rb2 [0.1652 (6), 0.25, 0.5778 (5)] and S [0.224 (2), 0.25, 0.889 (1)]. The diffraction pattern at 0.7 GPa is shown in Fig. 2 together with the calculated pattern of the refined model to illustrate the quality of the refinement. The refined parameters were: the overall scale factor, the cell parameters, the pseudo-Voigt profile function with terms to account for the reflection anisotropic broadening, the fractional atomic coordinates and a March–Dollase preferred orientation correction for the (1 1 2) plane. The background was substracted manually and not refined. During the refinement process, displacement factors were physically meaningless. For this reason, the overall displacement parameter was fixed at $B = 0.05$ Å^2, as in other similar compounds.

The anticotunnite structure of phase II is shown in Fig. 3. This transition was expected for the Rb_2S compound, because:

(i) this structural sequence had been observed in Li_2S (Grzechnik *et al.*, 2000) and Na_2S (Vegas *et al.*, 2001), and

(ii) Cs_2S (Sommer & Hoppe, 1977) and RbKS (Sabrowsky & Vogt, 1992) are anticotunnite-type at atmospheric pressure. The anticotunnite structure is typically described as chains of trigonal prisms of alkali atoms, in this case Rb atoms, connected by common edges and running parallel to the *ac* plane (see Fig. 3; O'Keeffe & Hyde, 1985). The S atoms center these Rb_6 trigonal prisms where each S atom is surrounded by nine Rb atoms, six of them corresponding to the apices of the prism and three extra Rb atoms belonging to adjacent chains, which cap the lateral faces of the prism (see Fig. 2). The interatomic Rb—S distances are collected in Table 1.

The evolution observed for the unit-cell volumes of the different phases is shown in Fig. 4. There it can be seen that the anticotunnite phase is stable up to at least 2 GPa. The variation of the volumes with pressure could be fitted to a third-order Birch–Murnaghan equation-of-state (EOS; Birch, 1978), where the values of the bulk modulus (B_0) and the atomic volume at zero pressure (V_0) are left to vary freely and B_0' is fixed to 4. The characteristic parameters obtained for the *anti*-$PbCl_2$-type phase are: $V_0 = 430 \pm 2$ Å^3 and $B_0 = 12 \pm 1$ GPa. This experimental value is in good agreement with the theoretical reported value: $B_0 = 14.4$ GPa (Schön *et al.*, 2004), using Hartree–Fock calculations.

The lattice parameters of this orthorhombic phase decrease continuously with pressure. For instance, the absolute contractions for *a*, *b* and *c* between 0.7 and 2 GPa are 0.241, 0.117 and 0.193 Å. However, when analysed in relative terms, these variations are 2.95, 2.3 and 1.94%, indicating that the compression is relatively isotropic.

Upon further compression additional peaks appear in the X-ray patterns and the diffraction peaks of phase II gradually lose intensity. These facts indicate the onset of a gradual phase transition to a phase we will denote as phase III. We could not identify the phase or phases occurring between 2.6 and 4.5 GPa. The transition to phase III is completed at 4.5 GPa; phase III is stable up to the maximum pressure reached in this experiment, 8 GPa. The pattern for the sample at 5.1 GPa upon compression (Fig. 5) could be indexed on the basis of an hexagonal cell with $a = 5.31$ (1), $c =$

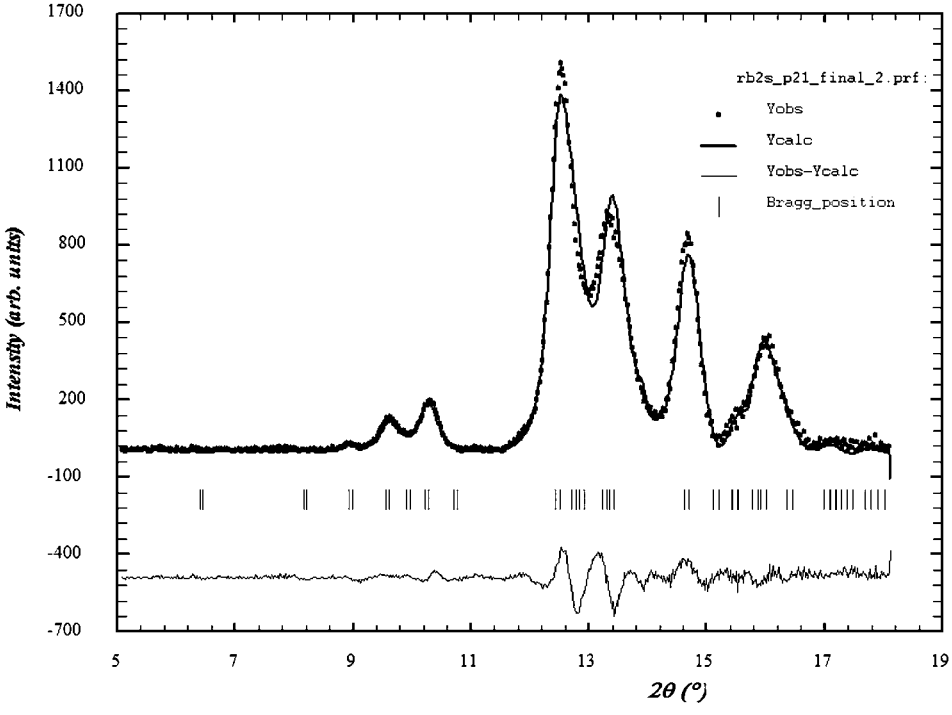

Figure 2
Observed, calculated and difference X-ray diffraction profiles of orthorhombic Rb_2S at 0.7 GPa (phase II). Vertical markers indicate Bragg reflections. The R_{Bragg}, R_{wp} and R_p residuals, whose definitions are given in the *FULLPROF* manual (Rodriguez-Carvajal, 1993), are 0.0146, 0.089 and 0.0653.

6.81 (1) Å, V = 166.3 (3) Å^3, Z = 2. This diagram is in fact very similar to that of the Ni_2In-type phase in Na_2S, with space group $P6_3/mmc$. The systematic absences are consistent with this space group and the refinement of the Ni_2In structure model matches the experimental diagram very well (see Fig. 5). In this case the number of parameters refined was the same as in the phase II refinement, except that now the atom coordinates are fixed at the Wyckoff sites 2*a*, 2*c* and 2*d*, *i.e.* Rb1 at 2*a* (0, 0, 0), Rb2 atoms at 2*d* (1/3, 2/3, 3/4) and S atoms at 2*c* (1/3, 2/3, 1/4). A March–Dollase preferred orientation correction for the (110) plane was also used. The refinement and experimental details of the two high-pressure phases are collected in Table 2.

The Ni_2In-type structure of phase III is represented in Fig. 6. This transition was also expected to occur for Rb_2S, because the hexagonal Ni_2In structure had been observed in Na_2S at 16 GPa (Vegas *et al.*, 2001) and a slight orthorhombic distortion was found in K_2S at 6 GPa (Vegas *et al.*, 2002). Moreover, it is well known that heavier elements, going down a column in the periodic table, tend to adopt the high-pressure structures of their parent lighter elements at lower pressures. Thus, it should be expected that in Rb_2S such a transition occurs at lower pressures than in Na_2S and K_2S.

The Ni_2In-type structure is usually described as straight chains of trigonal prisms (in this case formed by Rb atoms), connected by common edges and running parallel to the *ac* plane (see Fig. 6; O'Keeffe & Hyde, 1985). The S atoms center these Rb_6 trigonal prisms in such a way that each S atom is surrounded by 11 Rb atoms, six of them corresponding to the apices of the prism and five extra Rb atoms belonging to adjacent chains (see these five additional contacts in Fig. 5). The interatomic Rb—S distances at 5.1 GPa are collected in Table 1. From this table it can be inferred that the mean Rb—S distance in the trigonal prism is almost constant with pressure (3.497 and 3.507 Å for the *anti*-$PbCl_2$ and Ni_2In phases). This can be explained looking at the distortion of the trigonal prisms which, in the Ni_2In phase, have a smaller triangular face (Rb—Rb distances of 1 × 3.405 Å and 2 × 3.507 Å) and it is considerably higher (Rb—Rb distance of 5.31 Å) than that of the *anti*-$PbCl_2$ phase (triangular sides of 4.006, 4.049 and 4.26 Å, and a height of 5.101 Å).

In 2007 Vegas and Garcia-Baonza proposed a different structural description based on the Zintl–Klemm (*ZK*) concept that gave a rational explanation for the existence of the Ni_2In structure (Vegas & García-Baonza, 2007). This structure could be directly derived from that of NiAs. Thus, NiAs can be described as a simple hexagonal array of Ni atoms with one half of the trigonal prisms occupied by As atoms. If the empty trigonal bipyramids are filled by additional (Ni) atoms, the Ni_2In structure is produced. Such filling leads to a structure in which *h.c.p.* layers of Ni atoms alternate with graphite-like layers formed by [NiIn] entities. This description of the structure interprets the Ni_2In-type structure as a superstructure of the AlB_2-type, as reported by Zheng & Hoffmann (1989). The Ni_2In-type structure of Rb_2S can be understood in the light of the extended *ZK* concept (*EZK*; Vegas & García-Baonza, 2007). If one assumes that the Rb1 atoms at (0,0,0) formally transfer one electron to the [Rb2—S] framework, it becomes Ψ-[SrS], a II–VI compound with a graphite-like (IV–IV) structure. If, on the contrary, the Rb2 atoms are thought to donate their valence electron to Rb1, then the [Rb1—S] moiety is converted into Ψ-[SrS] but with the NiAs-type. An alternative electron transfer is from Rb2 atoms to the S atoms. In this case, a Ψ-[RbCl] arrangement is formed. This structure, unknown for alkali halides, is known for $LiClO_4$ in the form of the related, orthorhombically

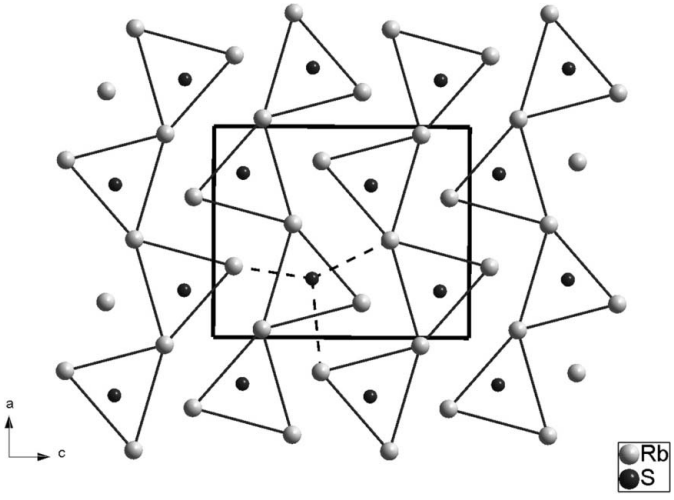

Figure 3
Crystal structure of anticotunnite Rb_2S (*Pnma*, Z = 4) at 0.7 GPa upon compression. Light and dark grey circles are the Rb and S atoms. The structure is projected along **b** and shows the walls of trigonal prisms of Rb atoms, which are occupied by S atoms, connected by common edges. Alternate walls are shifted by *b*/2. The S atoms are coordinated by nine Rb atoms, six of them corresponding to the apices of the prism and three extra Rb atoms belonging to adjacent chains (dashed lines).

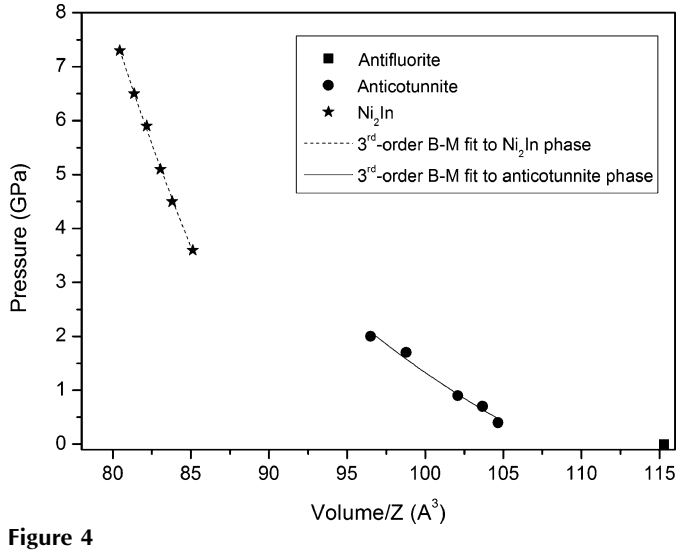

Figure 4
Pressure dependence of the unit-cell volumes of the different phases of Rb_2S. As shown in the insert, solid squares, circles and stars represent V–P data points corresponding to the antifluorite-, anticotunnite and Ni_2In-type phases, respectively. The EOSs fitted are also illustrated as solid and dashed lines for the anticotunnite-type and the Ni_2In-type phases.

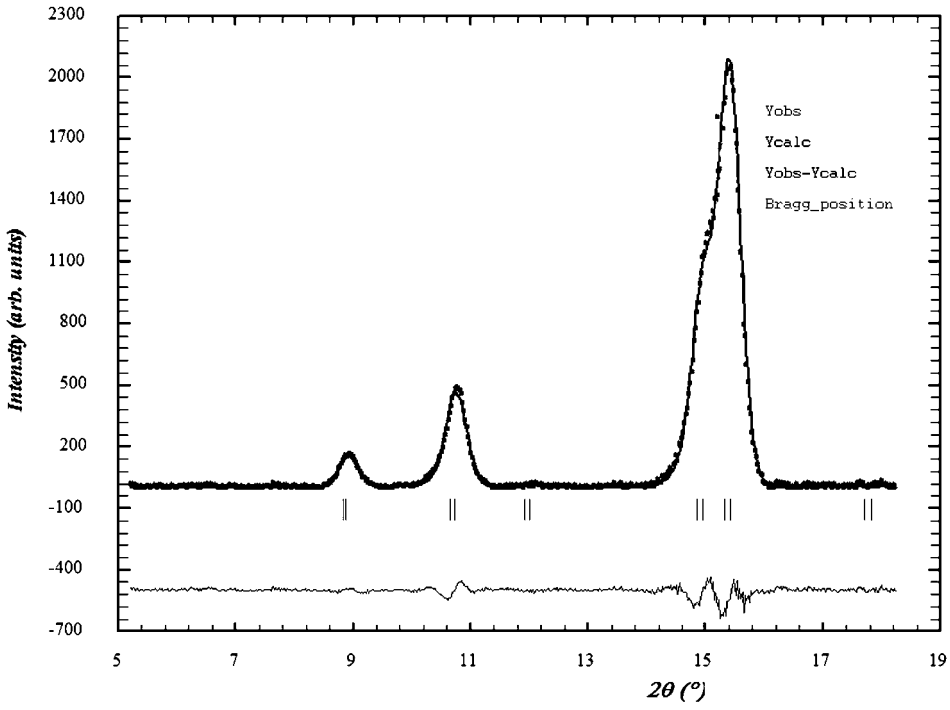

Figure 5
Observed, calculated and difference X-ray diffraction profiles of hexagonal Rb_2S at 5.1 GPa (phase III). Vertical markers indicate Bragg reflections. The R_{Bragg}, R_{wp} and R_p residuals are 0.0262, 0.154 and 0.075.

The bulk modulus (B_0) and the volume at zero pressure (V_0) obtained for the Ni_2In-type phase when B_0' is fixed to 4 are B_0 = 33 ± 1 GPa and V_0 = 181.5 ± 0.3 Å^3 (see Fig. 4). This value of B_0 is in good agreement with that predicted by *ab initio* calculations (Schön *et al.*, 2004), B_0 = 33.1 GPa using DFT–LDA–PWGGA (density functional theory–local density approximation–Perdew–Wang generalized gradient approximation). The lattice parameters *a* and *c* of this hexagonal phase contract 0.085 (1.6%) and 0.165 Å (2.4%), showing a slight anisotropic compression. The volume collapse in the transformation *anti*-$PbCl_2$-type to Ni_2In-type can be estimated in approximately 8%.

It is also important to point out that these two observed high-pressure phase transitions were successfully predicted using Hartree–Fock calculations (Schön *et al.*, 2004). The *anti*-CaF_2 → *anti*-$PbCl_2$ transition was predicted at *ca* 1.9 GPa and the Ni_2In-type structure at *ca* 4.5 GPa, in good agreement with our experimental results. These calculations led to a third high-pressure candidate. The structure should be stable above 18 GPa (Schön *et al.*, 2004), with an orthorhombic cell, space group *Fddd*, but whose structure-type could not be identified. Now we know that this distorted $CuSO_4$-type as reported by Wickleder (2003). The conclusion is that phase III of Rb_2S may be considered an intergrowth of two structures, *i.e.* the Rb-stuffed NiAs-type and the AlB_2-type.

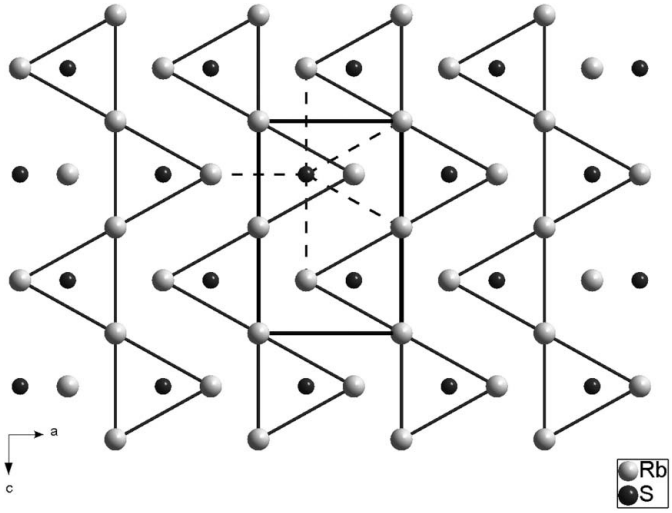

Figure 6
The crystal structure of the second high-pressure phase of Rb_2S ($P6_3/mmc$, Z = 2) at 5.1 GPa, projected along the *b* axis. As in Fig. 3, light and dark grey circles represent Rb and S atoms. Its Ni_2In-type structure has been outlined by drawing the Rb—Rb contacts forming the trigonal prisms where the S atoms are inserted. The S atoms are coordinated by 11 Rb atoms, six of them corresponding to the apices of the prism and five extra Rb atoms belonging to adjacent chains (dashed lines). These adjacent chains of trigonal prisms are shifted by half the projection axis.

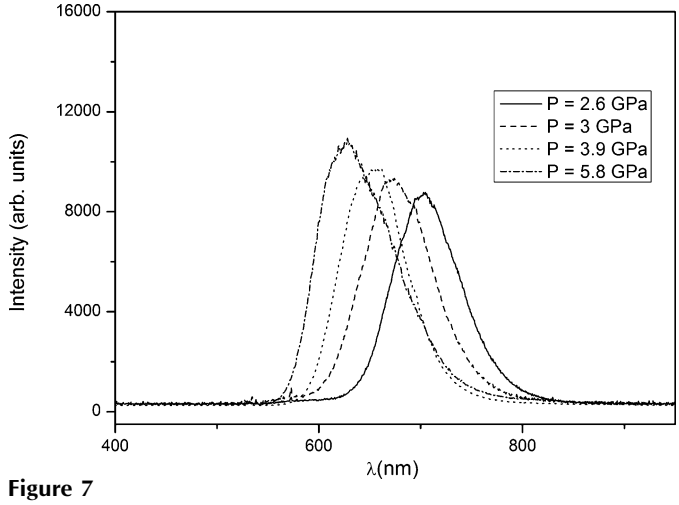

Figure 7
Series of luminescence spectra of the Rb_2S sample at different pressures. Strong luminescence is only observed above 2.6 GPa (band maximum at 703 nm) when the transition to the Ni_2In-type phase starts to occur, the band maximum showing a non-linear blue shift with pressure. Emitted intensities have been modified in order to compare more easily the shift of the maxima. The intensity of the emitted light is much higher when the transition to phase III is completed (above 4 GPa).

Table 2
Experimental details.

For all structures: Rb_2S, M_r = 203.00. Experiments were carried out at 293 K with Mo $K\alpha$ radiation, λ = 0.71073 Å using an Xcalibur Oxford Difraction diffractometer. Refinement was with 0 restraints.

	Phase III	Phase II
Crystal data		
Crystal system, space group	Hexagonal, $P6_3/mmc$	Orthorhombic, *Pnma*
a, b, c (Å)	5.30756 (8), 5.30756 (8), 6.80615 (4)	8.167 (10), 5.101 (6), 9.957 (11)
α, β, γ (°)	90, 90, 120	90, 90, 90
V (Å^3)	166.04 (1)	414.7 (8)
Z	2	4
μ (mm^{-1})	29.79	23.85
Specimen shape, size (mm)	Cylinder, 0.2 × 0.05	Cylinder, 0.2 × 0.05
Data collection		
Specimen mounting	Diamond–anvil cell	Diamond–anvil cell
Data collection mode	Transmission	Transmission
Scan method	φ	φ
2θ values (°)	$2\theta_{min}$ = 5.234, $2\theta_{max}$ = 18.304, $2\theta_{step}$ = 0.024	$2\theta_{min}$ = 5.067, $2\theta_{max}$ = 18.927, $2\theta_{step}$ = 0.024
Refinement		
R factors and goodness of fit	R_p = 0.082, R_{wp} = 0.193, R_{exp} = 0.085, R_{Bragg} = 0.026, χ^2 = 5.219	R_p = 0.091, R_{wp} = 0.159, R_{exp} = 0.073, R_{Bragg} = 0.016, χ^2 = 4.685
No. of data points	547	580
No. of parameters	8	14

Computer programs: *FULLPROF* (Rodríguez-Carvajal, 1993).

Table 3
Structures of the alkali sulfides and the cation subarrays in their corresponding oxides (sulfates and sulfites).

HP denotes high-pressure phases, HT high-temperature phases, and RP and RT room-pressure and room-temperature, respectively.

Antifluorite (*anti*-CaF_2)	Anticotunnite (*anti*-$PbCl_2$)	Ni_2In	Anti-$TiSi_2$
Li_2S (RP-RT) Li_2SO_4 (RP-HT)	Li_2S (HP-RT)	d-Li_2SO_4 (HP-RT)	
Na_2S (RP-RT)	Na_2S (HP-RT)	Na_2S (HP-RT)	Na_2SO_4 (RP-RT)
		d-Na_2SO_3 (RP-RT)	
		Na_2SO_4 (RP-HT)	
K_2S (RP-RT)	K_2SO_4 (RP-RT)	K_2S (HP-RT)	
		d-K_2SO_3 (RP-RT)	
		K_2SO_4 (RP-HT)	
Rb_2S (RP-RT)	Rb_2S (HP-RT)	Rb_2S (HP-RT)	
	Rb_2SO_4 (RP-RT)	K_2SO_4 (RP-HT)	
	Cs_2S (RP-RT) Cs_2SO_4 (RP-RT)	Cs_2SO_4 (RP-HT)	

structure coincides with that of the Na_2S subarray in thenardite V-Na_2SO_4, both being of the $TiSi_2$-type as observed by Ilyushin *et al.* (2004). Later, Vegas and García-Baonza found out that this structure would be of the $TiSi_2$-type and suggested the following 'universal' high-pressure sequence for the A_2B compounds (Vegas & García-Baonza, 2007)

antifluorite → anticotunnite → Ni_2In-type → $TiSi_2$-type → $MgCu_2$-type (Laves phase).

Further high-pressure experiments to observe the $TiSi_2$-type phase of Rb_2S are scheduled.

The Ni_2In-type structure of Rb_2S is stable up to 8 GPa, the maximum pressure reached in our experiments. In the decompression process, Rb_2S gradually transforms from the Ni_2In (phase III) into the anticotunnite-type phase (phase II) in the pressure range 3.6–1.7 GPa, showing a small hysteresis compared with the compression experiment. Phase II is restored at 1.7 GPa. At 0.4 GPa the sample still presents an anticotunnite-type structure. Further decompression led to the reaction of the sample with air, instead of recovering the antifluorite-type structure. Therefore, it was impossible to verify whether the *anti*-CaF_2-type structure would be recovered at room pressure or not.

At this point it is important to note a remarkable fact observed upon compression. That is, the strong luminescence observed above 2.6 GPa when the sample was excited with the 532 nm laser used for pressure determination. This luminescence only appears above 2.6 GPa (band maximum at 703 nm) when the transition to the Ni_2In-type phase starts to occur, the band maximum showing a non-linear blue shift with pressure (see Figs. 7 and 8). However, when the transition to the Ni_2In-type structure is completed, the blue shift of the emission maxima seems to follow a linear behaviour, with a constant displacement of 13.5 nm GPa^{-1}. The intensity of the emitted light increases significantly up to the pressure where the sample completely transforms into phase III. The shape of the emitted peak deviates from a Gaussian profile with pressure, showing an important anisotropic broadening component.

Another interesting aspect related to the high-pressure phases of Rb_2S is that they adopt the same structures as the cation arrays of the corresponding oxide Rb_2SO_4 at different conditions. Thus, phase II with the anticotunnite structure presents the same cation array as that of the ambient-pressure phase of Rb_2SO_4 (Ogg, 1928). At high temperatures of *ca* 930 K rubidium sulfate undergoes a phase transition to a hexagonal polymorph ($P6_3/mmc$; Fischmeister, 1962). The cation array of this new phase is of the Ni_2In-type, just like the arrangement found in the HP phase III of Rb_2S described here. Similar relationships between the structures of other alkali sulfides and the cation subarray in their corresponding oxides were firstly pointed out by O'Keeffe & Hyde (1985)

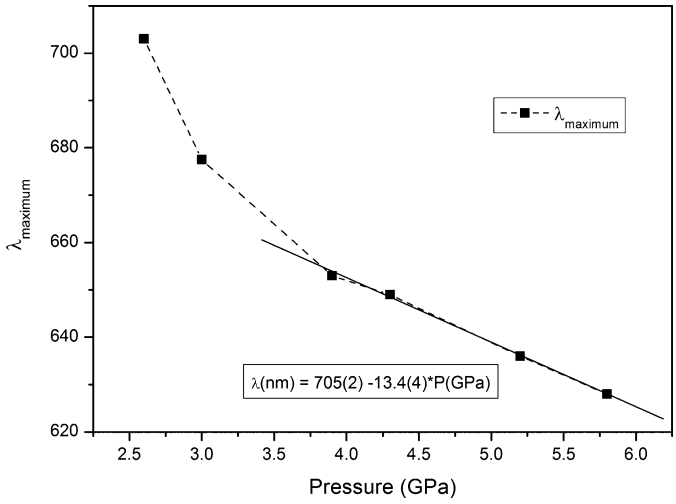

Figure 8
Evolution of the position of the luminescence maxima with pressure. At ~ 4 GPa, when the transition to the Ni_2In-type structure is completed, the blue shift is approximately constant, with a value of 13.5 nm GPa^{-1}.

and later by Vegas *et al.* for the pairs Li_2S/Li_2SO_4, Na_2S/Na_2SO_4 and Cs_2S/Cs_2SO_4 (Grzechnik *et al.*, 2000; Vegas *et al.*, 2001, 2002; Vegas & Jansen, 2002). All these similarities are collected in Table 3, in which each compound is allocated in its corresponding structure type of the above-mentioned high-pressure sequence in agreement with the model which relates oxidation and pressure (Vegas & Jansen, 2002).

4. Concluding remarks

A very air-sensitive Rb_2S powder was synthesized by heating stoichiometric amounts of the constituent elements. High-pressure ADXRD measurements on the initial antifluorite Rb_2S compound indicate two structural phase transitions above 0.7 GPa and 4.5 GPa to an anticotunnite and a Ni_2In-type structure. Upon decompression, the anticotunnite-type phase is fully reversible at 1.7 GPa, decomposing at atmospheric pressure owing to reaction with air. The new high-pressure phases, the transition pressures and their EOSs are in excellent agreement with previous theoretical calculations based on an investigation of the global enthalpy landscape, and subsequent Hartree–Fock and LDA optimizations. In addition, the two high-pressure Rb_2S phases, anticotunnite and Ni_2In-type, are similar to the cation subarrays of the phases of Rb_2SO_4 at room and high temperature. This compound is a new example of structural similarity between the substructure of oxides and the structure of the corresponding intermetallic compounds (Vegas *et al.*, 2001, 2002; Vegas & Jansen, 2002; Santamaría-Pérez & Liebau, 2010; Santamaría-Pérez & Vegas, 2003; Santamaría-Pérez *et al.*, 2005).

Together with the second high-pressure phase transition, the appearance of a strong luminescence is observed when excited with a green laser. The reasons for this surprising phenomenon remain unknown.

DSP acknowledges the financial support from Spanish MICCIN under project CTQ2009-14596-C02-01 as well as from Comunidad de Madrid and the European Social Fund S2009/PPQ-1551 4161893 (QUIMAPRES).

References

Beck, H. P. (1979). *Z. Anorg. Allg. Chem.* **459**, 72–80.
Birch, F. (1978). *J. Geophys. Res.* **83**, 1257–1268.
Brixner, L. H. (1976). *Mater. Res. Bull.* **11**, 1453–1456.
Duclos, S. J., Vohra, Y. K., Ruoff, A. L., Jayaraman, A. & Espinosa, G. P. (1988). *Phys. Rev. B*, **38**, 7755–7758.
Errandonea, D., Santamaría-Pérez, D., Bondarenko, T. & Khyzhun, O. (2010). *Mater. Res. Bull.* **45**, 1732–1735.
Fischmeister, H. F. (1962). *Monatsh. Chem.* **93**, 420–424.
Grzechnik, A., Vegas, A., Syassen, K., Loa, I., Hanfland, M. & Jansen, M. (2000). *J. Solid State Chem.* **154**, 603–611.
Ilyushin, G. D., Blatov, V. A. & Zakutkin, Y. A. (2004). *Z. Kristallogr.* **219**, 468–478.
López-Solano, J., Rodríguez-Hernández, P., Muñoz, A., Gomis, O., Santamaría-Pérez, D., Errandonea, D., Manjón, F. J., Kumar, R. S., Stavrou, E. & Raptis, C. (2010). *Phys. Rev. B*, **81**, 1441269.
Mao, H. K., Xu, J. & Bell, P. M. (1986). *J. Geophys. Res. B Solid Earth Planets*, **91**, 4673–4676.
May, K. (1936). *Z. Kristallogr.* **94**, 412–413.
Nolze, G. & Kraus, W. (1998). *Powder Diffr.* **13**, 256–259.
Ogg, A. (1928). *Philos. Mag.* **5**, 354.
O'Keeffe, M. & Hyde, B. G. (1985). *Struct. Bond.* **61**, 77–144.
Rodríguez-Carvajal, J. (1993). *Physica B*, **192**, 55–69.
Sabrowsky, H. & Vogt, P. (1992). *Z. Anorg. Allg. Chem.* **616**, 183–185.
Santamaría-Pérez, D. & Liebau, F. (2010). *Struct. Bond.*, doi: 10.1007/430_2010_27.
Santamaría-Pérez, D. & Vegas, A. (2003). *Acta Cryst.* B**59**, 305–323.
Santamaría-Pérez, D., Vegas, A. & Liebau, F. (2005). *Struct. Bond.* **118**, 121–177.
Schön, J. C., Cancarević, Z. & Jansen, M. (2004). *J. Chem. Phys.* **121**, 2289–2304.
Sommer, H. & Hoppe, R. (1977). *Z. Anorg. Allg. Chem.* **429**, 118–130.
Vegas, A. & García-Baonza, V. (2007). *Acta Cryst.* B**63**, 339–345.
Vegas, A., Grzechnik, A., Hanfland, M., Muhle, C. & Jansen, M. (2002). *Solid State Sci.* **4**, 1077–1081.
Vegas, A., Grzechnik, A., Syassen, K., Loa, I., Hanfland, M. & Jansen, M. (2001). *Acta Cryst.* B**57**, 151–156.
Vegas, A. & Jansen, M. (2002). *Acta Cryst.* B**58**, 38–51.
Wickleder, M. S. (2003). *Z. Anorg. Allg. Chem.* **626**, 1468–1472.
Zheng, C. & Hoffmann, R. (1989). *Inorg. Chem.* **28**, 1074–1080.
Zintl, E., Harder, A. & Dauth, B. (1934). *Z. Elektrochem.* **40**, 588–593.